Direct identification of fracture parameters of wood in mode I by digital image correlation

O Cochet, Jose Xavier, Rui F Martins, Rostand Moutou Pitti

Available online at www.sciencedirect.com

ScienceDirect

Structural Integrity Procedia 00 (2022) 000–000

Structural Integrity Procedia

www.elsevier.com/locate/procedia

ICSI 2023 The 5th International Conference on Structural Integrity

Direct identification of fracture parameters of wood in mode I by digital image correlation

O. Cochet[a], J. Xavier[b,*], R.F. Martins[b], R. Moutou Pitti[a]

[a] *Université Clermont Auvergne, Clermont Auvergne INP, Institut Pascal, Clermont-Ferrand, France*

[b] *UNIDEMI, Department of Mechanical and Industrial Engineering, NOVA School of Science and Technology, NOVA University Lisbon, 2829-516 Caparica, Portugal*

Abstract

Wood is an increasingly popular engineering material due to its potential for reducing pollution and combating global warming. Its use in construction has been recognised as a promising solution for sustainable and efficient building design. However, ensuring the safety and reliability of wooden structures requires a comprehensive understanding of the fracture mechanics of wood. In this study, we investigate the cracking behaviour of softwood species using MMCG specimens. We aim to accurately determine crack length during fracture propagation and related fracture parameters, which is often challenging to obtain in wood. To achieve this, we employ the Arcan system to load the specimen, which has the advantage of inspecting from pure to mixed mode fracture loading to activate different failure modes. Digital Image Correlation (DIC) measures displacement and strain fields near the crack. Our primary focus is on open I mode crack growth, and we generate force versus crack opening curves from the measurements. In addition, we use the imposed displacement compliance method to determine the strain energy release rate for opening mode. This study highlights the importance of fracture mechanics in ensuring the safety and reliability of wooden structures. Knowledge of the fracture parameters of wood can aid in the design and development of more efficient and sustainable wooden products. Accurate determination of crack length is critical in this regard. Therefore, using digital image correlation techniques and imposed displacement compliance methods can improve our understanding of the fracture behaviour of wood and aid in the design of more reliable and efficient wooden structures.

Keywords: Digital image correlation; Mode I; Fracture parameters

Nomenclature

A radius of

* Corresponding author. Tel.: +351 212 948 567.
E-mail address: jmc.xavier@fct.unl.pt

B position of
C further nomenclature continues down the page inside the text box

1. Introduction

Wood is a natural resource present on all continents. In France, it represents 15 million hectares and 3.3 million hectares in Portugal. It is a natural, renewable, low energy cost, recyclable and biologically degradable material. Today, global warming is a significant concern and using wood in the construction sector would make it less polluting. It is used for many applications. It can be used as energy, in timber frames and constructions, for packaging, furniture and joinery, in the paper industry or the chemical industry, for example. In addition, the cost of wood is one of the lowest. However, the mechanical behavior of wood, and more specifically its failure properties needs to be more studied in order to design reliable structures. This lack of study may lead for instance to the sudden failure of structures during their service life, which is not acceptable. Studying the failure properties of wood is therefore crucial to guide local engineers in their choice of building materials other than concrete and steel. One of the defects of wood is its natural origin. This gives it a great source of variability in its characteristics. It is subject to weathering and, depending on the climatic conditions, it will not have the same properties. This is why it must often be used after a specific treatment. The present document aims to study mechanical fracture of wood in mode I on silver fir specimens of type 2MCG. The proposed work consists mainly in conducting measurements carried out by kinematic field measurements obtained by the method known as image correlation or DIC. Integrating the DIC method through the MatchID software and subsequent Python-based data processing will be instrumental in attaining the desired outcomes. Two Python programs will be compared in order to verify the acuity of each method. This project consists of modelling the observed behaviour, both from the crack initiation and propagation point of view. The study will focus solely on a single wood species, and variations in wood moisture content will not be considered. The tests were carried out in a universal testing machine with a homemade Arcan fixture. This data can be used in future studies to develop computational simulations of fracture testing to determine fracture parameters from inverse methods.

2. Methods

2.1. Material and testing

The MMCG specimen was initially developed by R. Moutou Pitti (2008). This sample is a compromise between DCB and CTS samples to obtain different mixing rates and a stable crack propagation. The choice was made regarding to the good stability of the crack propagation. The Geometry, visible on Figure 1 was already tested in (Odounga) works.

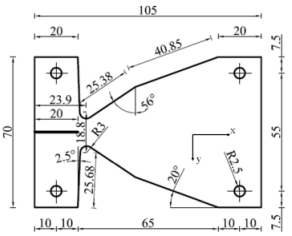

Fig. 1: dimensions and geometry of Mixed Mode Crack Growth specimen

.

For the tests, the chosen European species is the silver fir, which belongs to the category of coniferous trees. This softwood species is predominantly found in the northern hemisphere, similar to pines and other aged trees. Its name

originates from the white colour of its wood, and its circumference typically ranges from 50 to 80 cm. According to CIRAD data, the silver fir exhibits a density of 0.45 to 0.60, a saturation fiber point (SFP) of approximately 30%, and a compressive strength of 41 MPa. Wooden specimens were carefully characterised before testing by measuring weight, density, and moisture content. Before the tests, the samples were weighed, denoted as M_H, to determine their mass during testing. The wood density can also be derived from the sample's volume and mass. The density of each sample can be determined by applying the formula $\rho = M/V$. After testing, the specimens were placed in an oven set at 100 degrees until their mass, labelled as M_C, stabilised. Two specimens were subjected to this process for 73 hours, and various measurements were taken until a constant mass was achieved. The moisture content of the specimens can be determined using equation 1. Consequently, we possess the average mass M_H of 29.83g, the density of 431.3kg/m^3, and the moisture content of 10.3%.

$$HI(\%) = \frac{M_H - M_0}{M_0} \tag{1}$$

An Arcan fixture system is required to perform the 2MCG fracture tests. Indeed, this part allows the connection of the 2MCG wood specimen (Figure 1) to the cross-head displacement of the test frame. Figure 2 shows the Arcan device we will use, inspired by the thesis of (Odounga).

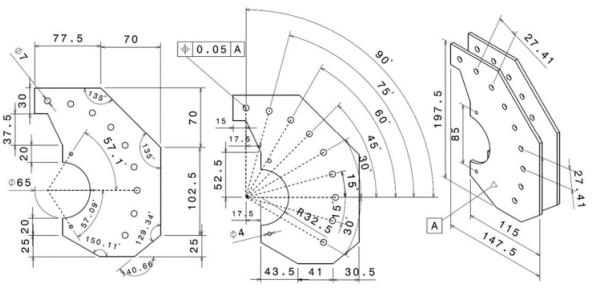

Fig. 2: Size of the Arcan fastening system (Odounga).

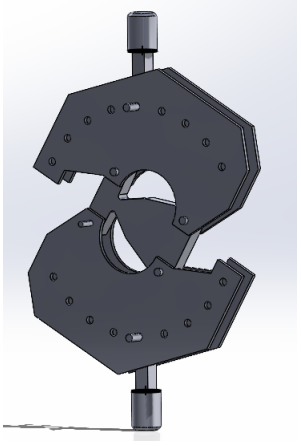

Fig. 3: Assembled device in Solidworks.

The fixing holes enables to load the specimen with different angular values of the angle in relation to the vertical direction in order to activate different failure modes depending on the load angle. The fixture was designed and assembled using SolidWorks software, and detailed technical drawings were produced for manufacturing (Figure 3).

2.2. *Optical set-up and settings*

The fracture tests were performed using a Landmark Servohydraulic testing machine with a maximum capacity of 100 kN. Figure 4 shows the experimental set-up, which includes the Arcan fixture and the optical camera-lens-illumination devices. The Arcan fixture was mounted to the testing machine using standard bolts, with washers inserted between the specimen and the Arcan system to reinforce the attachment points. To facilitate specimen changes between tests, manual controls were employed to elevate the moving part of the testing machine, minimising residual tension between the bolt holes and the Arcan system. Furthermore, before testing, an arbitrary pre-load was applied to the specimen to prevent any clearance or unintended movement of the specimen (which could cause image defocusing). Load and cross-head displacement data were recorded at a frequency of 5 Hz . Additionally, a real-time plot was generated during the test for visualisation.

An Alvium 1800 U-2040m Allied Vision camera and a 60 mm Nikkor lens were used for image grabbing and acquisition. The camera has a resolution of 4512 (H) × 4512 (V) and a sensor size of type 1.1. The front of the lens was positioned at a working distance of 285 mm with an aperture of f/11 and an exposure time of 60 milliseconds. The cross-head displacement of the testing machine was 0.02mm/s, and the camera had a frequency of 1 Hz (1 fps). A green illumination set-up was used to enhance the sensitivity of the sensor. Notably, care was taken during lens and camera adjustments to optimise focusing and exposure time, ensuring an appropriate spread of light intensity to prevent pixel saturation in the sensor. The camera was securely mounted on a tripod to ensure a stable position relative to the specimen's target surface, enabling the capture of consistent images throughout the tests. The frontal face of the specimens was coated with a suitable speckle pattern. A first layer of white paint was added and a cloud of black dots formed a second layer of paint to create a distinctive local pattern across the region of interest (ZOI) ahead of the crack tip.. Figure 5 shows an image of the speckle pattern, along with its corresponding image histogram. Additionally, a scale positioned in the surface plane was employed to establish the conversion factor for translating pixels into millimetres.

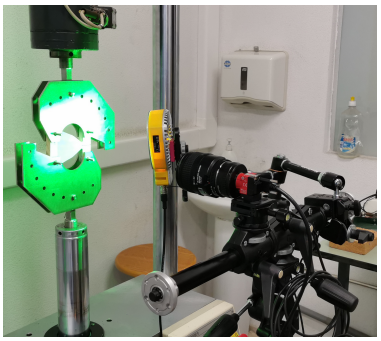

Fig. 4: Experimental set-up.

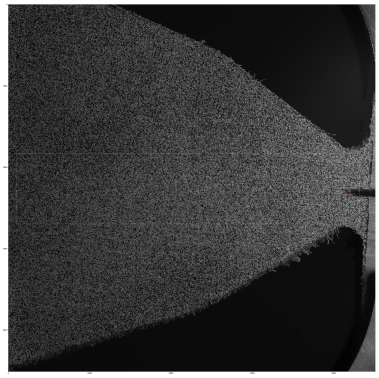

Fig. 5: Speckle pattern typically obtained with DIC Histogram of the speckle image.

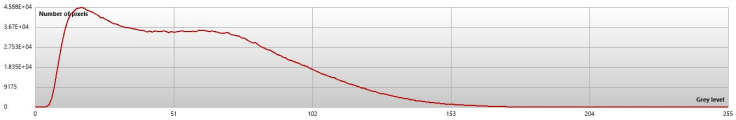

Fig. 6: Histogram of the speckle image.

2.3. Digital image correlation

Digital image correlation (DIC) was developed in 1983. It is a 2D or 3D optical method that measures displacements between two images. It enables the generation of displacement and strain maps, providing valuable kinematic information. The MatchID DIC 2D software was used in this study, and Python-based scripting was coded for post-processing purposes. The focus of this study was the evaluation of crack opening displacement and crack length variation during the fracture tests with regard to the applied load. In DIC processing, several steps are required:

- Choose a reference image that corresponds to the first image of the test
- Select multiple deformed images
- Define the zone of interest (ZOI) in which the crack propagates
- Define the DIC setting parameters
- Start the DIC analysis
- Exploit the results

It is important to highlight the significant impact of both extrinsic and intrinsic setup parameters in digital image correlation (DIC), including subset size, subset step, strain gauge window, shape functions, and correlation criterion (E.M.C. and Iadicola, 2018). These parameters play a crucial role in determining the accuracy and spatial resolution of the measured displacements and reconstructed strain fields (Xavier et al., 2012; Pereira et al., 2018). Consequently, they are considered fundamental factors. To achieve a trade-off between spatial resolution and accuracy, a parametric analysis was conducted utilizing the Parametric Module of MatchID. The resulting DIC settings are summarized in Table 1. It is believed that the pre-selected range of values is reflective of the permissible DIC setup parameter range.

Subsequently, data from each analysis were extracted in a matrix format for each acquisition step. These data were then subjected to further analysis using Python scripting, with the aim of evaluating fracture parameters within the scope of this study.

Parameter	**Setting**
Correlation Coefficient	ZNCC
Interpolation order	Bicubic Splines
Transformation order	Quadratic
Prefiltering	Gaussian
Progress history	Spatial
Subset size	31
Step size	10
Strain window size	5
Virtual Strain Gauge	71 pixels
Strain interpolation	Bilinear (Q4) Lagrange polynomials
Strain Convention	Green-Lagrange

Table 1: DIC setting parameters used in the MatchID software for the analyses.

2.4. Python code

2.4.1. Method 1: Crack propagation based on full-field displacement fields provided by DIC

The Crack Tip Opening Displacement (CTOD) is calculated by analysing subsets positioned just above and below the subset that initially defines the crack tip position (a_0) in the pre-crack propagation images (see Figure 7). The a_0 subset corresponds to a specific entry in row m and column n in matrix representation. Observing the subsets from top to bottom makes it possible to track the displacement of the crack tip and measure it accurately. The objective is to identify the most suitable pair of subsets sufficiently close to the crack for meaningful measurements without being too close or too far. Proximity to the crack ensures relevant information, while excessive proximity or distance may compromise the accuracy of measurements. Through the analysis of these displacements, the crack opening values at each step can be obtained.

The crack length evaluation is based on the variation of the relative position between adjacent subsets, which gives an estimate of the damage occurrence (Xavier, 2014). To begin with, a matching function A(x,y) 2 is determined based on the norm of the relative position vectors as follows:

$$A(x, y) = max(\|u_i - u_k\|; \|u_j - u_l\|) \tag{2}$$

where $u_{i,j,k,l}$ represent the displacement vector of four adjacent subsets. A mapping mask is then defined, assuming threshold segmentation according to the following inequalities.

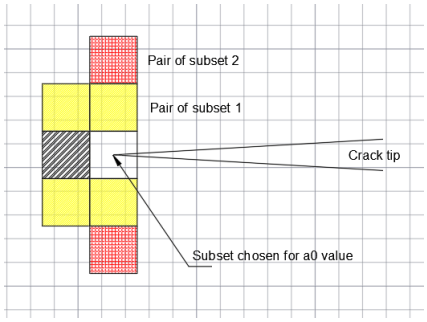

Fig. 7: Pair of subsets around the chosen subset a_0.

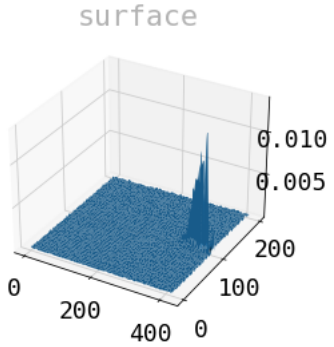

Fig. 8: A function

$$M(x,y) = \begin{cases} 1, & \text{if } A(x,y) \geq \alpha\overline{A} \\ 0, & \text{if } A(x,y) < \alpha\overline{A} \\ -1, & \text{if } A(x,y) = \text{NaN} \end{cases} \tag{3}$$

The matrix M serves as the basis for estimating the current horizontal location or crack length at a given stage. Zero values in the matrix indicate areas without a crack, while subsets within the crack or regions with missing information are assigned values of 1 and -1, respectively. Subsets surrounding the crack, which are of particular interest for the study, are assigned a value of 1. Constructing a sub-matrix consisting of -1, 0, and 1, one can visualise the damage evaluation as a map, providing an overview of the crack's development. Tracking the farthest subset with a value of 1 allows the determination of the last subset where the crack tip is located. To facilitate this, the parameter α acts as a cutoff tool, enabling the localisation of the crack position in the matrix coordinate space.

The selection of the α parameter is not straightforward in the initial approach. To approximate its value, we first seek a correlation factor using the least squares regression method. During the test, the load-displacement curve consists of three main regions: a linear region representing a stationary zone, a second region corresponding to fracture propagation, and a third region indicating specimen rupture. By determining the correlation factor, we can identify the stage between the stationary zone and the Fracture Process Zone (FPZ). A second verification criterion based on displacement field processing is then applied to confirm the correct stage of the FPZ. By following these two steps, we can determine the stage at which the FPZ begins and the possible range of values for α. Subsequently, we can plot the stages of crack propagation for different α values and assess the value of α that yields the largest $a(t)$ (crack length). Typically, the smallest α is chosen, unless a curve with simpler geometry is desired and the length of $a(t)$ remains relatively unchanged. A portion of the code enables graphical verification of the crack length by directly selecting a_0 and a_f in Python. This allows the elimination of certain α values that do not yield the correct crack length.

2.4.2. Method 2: Crack propagation based on crack opening displacement provided by DIC

Method 2 uses the crack opening along the entire length of the wooden specimen to determine the length of the crack (Filho et al., 2022).

From the reference and current positions of the DIC calculation points, the Euclidean distance between each pair of points can be measured and the COD can be determined as:

$$VD(k,i_n) = \sqrt{(x_{11bk} - x_{11tk})^2 + (x_{22bk} - x_{22tk})^2}_{i_n} - VD(k,i_0) \tag{4}$$

where the indices t and b refer to the DIC data points located at the top and bottom of the crack path, k is the index of the DIC point, i_n is the image captured at time n, $VD(k, i_0)$ is the initial Euclidean distance between the computational points of the top and bottom reference DIC subset obtained from image i_0, and x_{11} and x_{22} are their coordinates in the image plane. VD can be defined as a displacement gauge along the crack path 9.

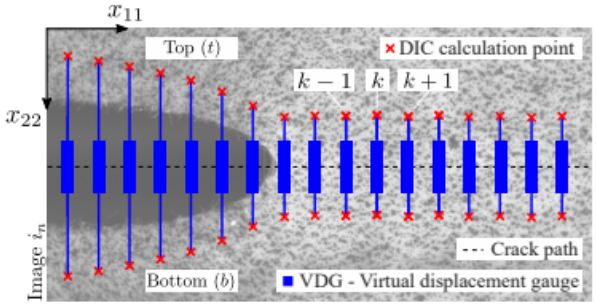

Fig. 9: DIC-based virtual displacement gauge (VDG) (Filho et al., 2022).

The first step towards detecting the crack tip is to take the average value of VD for each stage:

$$\overline{VD}(i_n) = \frac{1}{k}\sum_{k=1}^{k} VD(k, i_n) \tag{5}$$

The threshold value must be adjusted using the two parameters α and β which are obtained by solving the equation:

$$\begin{cases} VD_{th}(i_1) = \overline{VD}(i_1)(\alpha i_1 + \beta) \\ VD_{th}(i_f) = \overline{VD}(i_f)(\alpha i_f + \beta) \end{cases} \tag{6}$$

In order to obtain $VD_{th}(i_1)$ and $VD_{th}(i_f)$, it was first necessary to read graphically the position of the crack tip of the first and last image of the Fracture Process Zone and then to find the intersection between the position of the crack tip and the crack opening VD for those two stages.

Therefore, the adjusted threshold line-cut $VD_{th}(i_n)$ is given by:

$$VD_{th}(i_n) = \overline{VD}(i_n)(\alpha i_n + \beta) \tag{7}$$

The intersection between each $VD_{th}(i_n)$ and the corresponding $VD(k, i_n)$ curve at time n represents the x_{11} position of the crack tip, denoted by (p_n). It is therefore possible to calculate the growth of the crack at instant n:

$$da_n = p_n - p_0 \tag{8}$$

2.4.3. Energy release rate

After using one of the two previous methods, we can calculate the energy release rate in mode I. To determine the Energy release rate, compliance method was chosen. The formula used is written on 9:

$$G_{\mathrm{I}} = \frac{{F_c}^2}{2b}\,\frac{\partial C}{\partial a} \quad \text{with } C = \frac{v}{F_c} \tag{9}$$

With :
G_c the value of energy release rate (in J m^{-2})
F_c the critical force which involves the crack (in N)
b the thickness of the specimen (in mm)
∂C the compliance evolution (in $Pa^{-}1$)
∂a the crack length evolution (in mm)
v the crack opening displacement according to y

3. Results and Discussion

In the Figure 10, a characteristic load-displacement curve can be seen. Normally four distinct parts are observed on a load-displacement curve for Mode I fracture loading:

- A small area visible at the beginning of the curve which corresponds to the setting up of the loaded specimen.
- A nearly linear region arises from the elastic loading phase with a static crack front.
- The third segment is distinguished by a series of critical force peaks, which signify a distinct crack initiation. The progressive increase in these peaks confirms the crack's stability zone.
- Lastly, the final segment entails the material's rupture, which transpires when an ultimate force is applied, marking the instability of the crack.

It is followed by a plot of the crack lengths estimated by methods 1 and 2. The blue dots are crack lengths estimated graphically using Matchid and strain fields to check that the crack length estimated by Python is correct. Finally, the two other plots represent G with method 1 and 2 and show that G reaches a sort of plateau, corresponding to a stabilised propagation range.

Table 2 compares the maximum energy release rate values obtained in this study with those reported in the literature. The comparison focuses on temperate species with similar density, moisture content ranging between 9% and 12%, and an initial crack oriented in the radial-longitudinal (RL) direction. Silver fir's average maximum energy release rate is highlighted in bold and compared to different species and test methods, including 2MCG, DCB, and Wedge Splitting tests. Firstly, it is noteworthy that the magnitude of G for silver fir is within the same order of magnitude as other species. Silver fir exhibits a difference of 29% compared to alder, 36% compared to Pinus pinaster, and 33% compared to Padouk. Moreover, similar values have been reported in the work of Odounga (2018), albeit with a standard deviation 2 to 3 times greater, indicating more dispersed results. In the study by Xavier et al. (2014), experimental values of $G = 190$ J/m² were also obtained, which aligns with the results of this study. Additionally, alder and Pinus pinaster exhibit similar densities (around 0.1) in comparison to silver fir. The observed scattering of results can be attributed to the inherent material properties of wood, which is known for its high natural variability and anatomical composition. Furthermore, different energy release rate measurement methods and experimental parameter variations inevitably impact the final results. It is worth mentioning that the specimens in this study were predominantly derived from the extremity of the tree trunk rather than the central portion. The inclination of tree rings is apparent when observing our specimens, which could explain the slightly lower value obtained in our tests since $G_{RL} > G_{TL}$, as demonstrated in the article by Reiterer (2002).

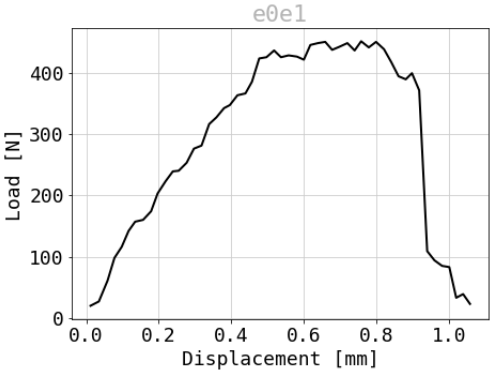

(a) P-Delta curve, for e0e1 specimen.

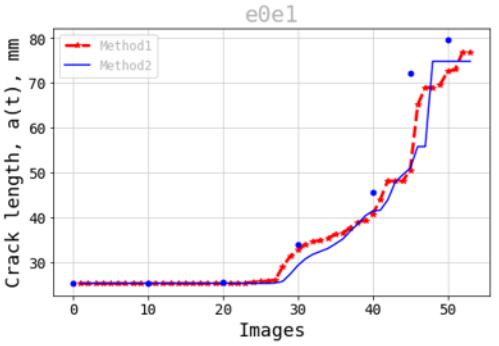

(b) Crack length depending on time, for e0e1 specimen.

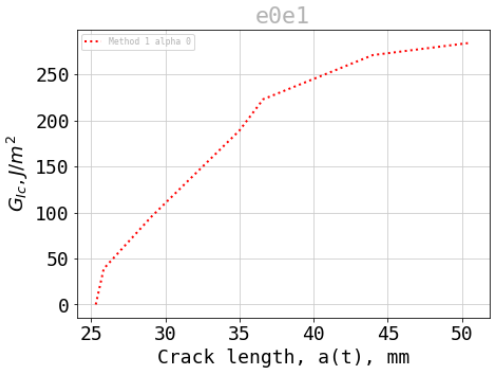

(c) Energy release rate depending on the crack length propagation method 1, for e0e1 specimen.

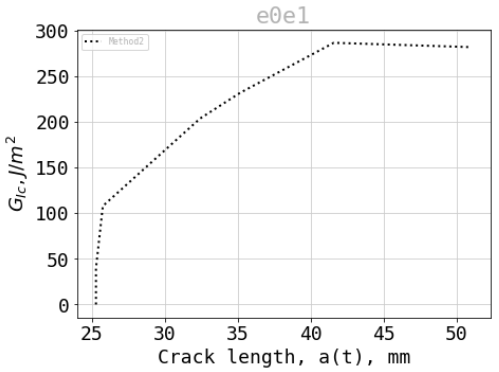

(d) Energy release rate depending on the crack length propagation method 2, for e0e1 specimen.

Fig. 10: Mechanical fracture characteristics of specimen e0e1

References	Wood species	Test type	Orientation	Density	$G_{\max}(J/m^2)$	Standard deviation
	Silver fir	**2MCG**	**RL**	**0.43**	**170**	**77**
(Angellier et al., 2017)	Douglas fir	DCB	RL	0.54	784	
Angellier et al. (2017)	White fir	DCB	RL	0.49	570	
(Xavier, 2014)	Pinus Pinaster	DCB	RL	0.543	270	64
(Reiterer et al., 2002)	Spruce	WS	RL	0.479	337	47
Reiterer et al. (2002)	Alder	WS	RL	0.510	244	41
Reiterer et al. (2002)	Oak	WS	RL	0.553	348	38
(Reiterer et al., 2002)	Ash	WS	RL	0.701	551	38
(Odounga)	Okoumé	2MCG	RL	0.39-0.5	317	160
(Odounga)	Iroko	2MCG	RL	0.56-0.7	323	200
(Odounga)	Padouk	2MCG	RL	0.7-0.88	255	200

Table 2: Comparison of mean max G values for specimens in the literature, 2MCG: Mixed Mode Crack Growth, DCB: Double Cantilever Beam, WS: Wedge Splitting test, RL: Radial Longitudinal.

4. Conclusions

In conclusion, this study aimed to investigate the fracture parameters of silver fir, a type of softwood species. The Arcan fixture was utilised to apply mode I fracture loading. Wooden specimens were specifically manufactured along the RL propagation planes. Digital image correlation (DIC) with MatchID software was employed to analyse the deformation patterns, and a Python code was developed for subsequent data processing to obtain fracture parameters, including crack tip opening displacement and crack length evaluation during the fracture tests. The experiments focused on open mode (mode I) tests conducted on MMCG specimens. The critical energy release rate for each specimen was calculated using the compliance method. Comparative analysis of the average G_{max} values with those of other temperate species revealed significant similarities, providing valuable insights into the fracture behaviour of silver fir. Moving forward, the geometry of the MMCG specimen, the Arcan system, and the developed Python code can be readily applied to future tests. It would be particularly intriguing to conduct tests in both mode I and mixed mode I+II using different wood species whilst also considering variations in humidity and temperature levels. Such comprehensive investigations would enhance our understanding of wood behaviour. However, it is important to acknowledge that due to the intricate nature of wood's behaviour, developing empirical models may be challenging, and each tested sample will likely exhibit unique characteristics. Therefore, numerous experiments are necessary to explore the complexities of this biological material.

4.1. General guidelines for the preparation of your text

Avoid hyphenation at the end of a line. Symbols denoting vectors and matrices should be indicated in bold type. Scalar variable names should normally be expressed using italics. Weights and measures should be expressed in SI units. All non-standard abbreviations or symbols must be defined when first mentioned, or a glossary provided.

Acknowledgements

This research was funded by the project UIDB/00667/2020 (UNIDEMI) supported by Fundação para a Ciência e a Tecnologia (FCT-MCTES), the Portuguese national funding agency for science, research and technology.

References

Angellier, N., Dubois, F., Pitti, R.M., Diakhaté, M., Loko, R.A., 2017. Influence of hygrothermal effects in the fracture process in wood under creep loading. Engineering fracture mechanics 177, 153–166.

E.M.C., Iadicola, M., 2018. A good practices guide for digital image correlation. International Digital Image Correlation Society doi:10.32720/idics/gpg.ed1.

Filho, J., Xavier, J., Nunes, L., 2022. An alternative digital image correlation-based experimental approach to estimate fracture parameters in fibrous soft materials. Switzerland: MDPI AG 15, 2413. URL: https://doi.org/10.3390/ma15072413.

Odounga, B., . Étude de la fissuration des bois tropicaux par mesures de champs.

Pereira, J., Xavier, J., Ghiassi, B., Lousada, J., Morais, J., 2018. On the identification of earlywood and latewood radial elastic modulus of pinus pinaster by digital image correlation: A parametric analysis. The Journal of Strain Analysis for Engineering Design 53, 566–574.

R. Moutou Pitti, F. Dubois, O.P., 2008. Sur une éprouvette assurant la stabilité de la propagation de fissure en mode mixte dans le matériau bois. Comptes rendus Mécanique 336, 744–749.

Reiterer, A., Sinn, G., Stanzl-Tschegg, S., 2002. Fracture characteristics of different wood species under mode i loading perpendicular to the grain. Mater Sci Eng A 332, 29–36.

Xavier, J., de Jesus, A., Morais, J., Pinto, J., 2012. Stereovision measurements on evaluating the modulus of elasticity of wood by compression tests parallel to the grain. Construction and Building Materials 26, 207–215.

Xavier, J.e.a., 2014. Direct evaluation of cohesive law in mode i of pinus pinaster by digital image correlation. Experimental Mechanics 54, 829–840.